A Quantum Mechanical Investigation of the Relation between Impact Sensitivity and the Charge Distribution in Energetic Molecules

Betsy M. Rice* and Jennifer J. Hare

U. S. Army Research Laboratory, Aberdeen Proving Ground, Maryland 21005

Received: July 10, 2001; In Final Form: October 26, 2001

Quantum mechanically determined electrostatic potentials for isosurfaces of electron density of a variety of CHNO explosive molecules are analyzed to identify features that are indicative of sensitivity to impact. This paper describes the development of models for prediction of impact sensitivity of CHNO explosives using approximations to the electrostatic potentials at bond midpoints, statistical parameters of these surface potentials, and the generalized interaction properties function [J. S. Murray, T. Brinck, P. Lane, K. Paulsen and P. Politzer, *J. Mol. Struct (THEOCHEM)* **1994**, *307*, 55] or calculated heats of detonation. The models are parametrized using a set of 34 polynitroaromatic and benzofuroxan explosives for which impact sensitivity measurements exist. The models are then applied to a test set of 15 CHNO explosives from a variety of chemical families in order to assess the predictive capability of the models. Patterns of the surface potentials of the molecules examined in this study suggest that the level of sensitivity to impact is related to the degree of positive charge buildup over covalent bonds within the inner framework of these explosives. The highly sensitive explosives show large positive charge buildup localized over covalent bonding regions of the molecular structures, whereas the insensitive explosives do not exhibit this feature. For the nitroaromatic and benzofuroxan compounds, sensitivity appears to be related to the degree and distribution of positive charge build-up localized over the aromatic ring or over the $C-NO_2$ bonds.

1. Introduction

A long-sought-after goal within the energetic materials community has been to develop capabilities to predict various properties of a notional energetic material that are associated with performance and sensitivity before expending resources in its synthesis. By achieving this goal, it is hoped that the development procedure for energetic materials would be improved. The current process is lengthy and expensive due to the heavy reliance on experimentation and measurement of a variety of candidate materials, from which only a few will be selected as most suitable to meet specified objectives. Therefore, this process has the potential for inordinate waste, particularly when developing and testing a material that turns out to be a poor candidate. Since the development, manufacture, testing, and fielding of a new energetic material is so costly in time and money, elimination of any poor candidate due to sensitivity or performance problems through predictive capabilities at the early stages of development is highly desirable.

In efforts to develop capabilities to predict the sensitivity of explosives, numerous studies have been performed that attempt to relate various molecular and bulk properties of explosives with their sensitivities to initiation.[1−34] Two problems with attempting to establish correlations between molecular properties and measured data arise with (1) the quality of the data used to establish the correlation and (2) finding enough data to establish a correlation. Reliable shock sensitivity tests exist, but the measurements using these tests have been performed for a relatively small number of pure explosives.[28,35] Thus, it is difficult to establish a correlation between molecular properties of pure explosives with such a small amount of data. On the other hand, there are many drop weight impact measurements for pure explosives.[28] The drop weight impact test is convenient and the most common method of assessing sensitivities, with the results indicating the ignitability of the explosive.[1] In this test, milligram quantities of an explosive sample are placed between a flat tool steel anvil and the flat surface of a tool striker.[1] Typically, a 2.5 kg weight is dropped from a predetermined height onto the striker plate, and the result (evidence of reaction or nonreaction) is recorded. A sequence of tests is carried out until the result, termed the $h_{50\%}$ value, is obtained. The $h_{50\%}$ value is the height from which 50% of the "drops" result in reaction of the sample. While the test itself is extremely easy to implement, the results are often not reproducible, and in some cases, the tests give widely varying $h_{50\%}$ values. For example, reported $h_{50\%}$ values for twice-recrystallized 2,4,6-trinitrotoluene (TNT) vary from below 100 to above 250 cm.[1,29] Because it is believed that hot spots in the material contribute to initiation in the drop weight impact test,[1,2,29,36,37] factors in the impact experiment that might affect the formation and growth of hot spots could strongly affect the measurements, making the results extremely sensitive to the conditions under which the tests are performed. Thus, the impact test is considered to provide only a crude, qualitative estimate of an explosive's sensitivity, and its results are often considered to be suspect. Additionally, there are questions as to whether the mechanisms for initiation under the impact hammer are the same as those involved in shock initiation.[1,28] However, the strong correlation between shock and impact sensitivity results provides a measure of justification to use drop weight impact tests as an indicator of the sensitivity of explosives to shock.[11,28] Despite all of the uncertainties associated with this test, there exist numerous impact measurements for pure explosives for use in studies such as presented here. Therefore, most of the studies that have attempted to associate molecular properties with sensitivities

10.1021/jp012602q
Published on Web 02/02/2002

rely on drop weight impact measurements.[1−34] Several simple relationships have been found that relate impact sensitivities with measured and predicted molecular properties, particularly within chemical families. These properties include the oxygen balance of the molecules,[1,2] molecular electronegativities,[8,9] vibrational states,[11,12] molecular weights and detonation gas concentrations,[6] parameters related to oxidation numbers,[10] partial atomic charges,[3−5,9,21,22] heats of reaction,[13,14] heats of explosion,[7] activation energies,[7,15−18,27] and bond orders.[15−17] While several of these studies have shown strong correlations between various molecular properties and impact sensitivity measurements, Brill and James showed that the existence of a large number of such correlations actually masks the underlying chemical mechanisms that dominate the initiation reactions upon impact and, thus, should not be used to interpret initiation mechanisms.[38] To illustrate this, they established 153 near-linear correlations between impact sensitivity and various electronic, molecular, and crystal properties for molecules in the amino-2,4,6-trinitrobenzene series. None of these correlations were helpful in identifying the early thermal decomposition reactions or the subsequent propagation reactions, which differ among these compounds and are assumed to play key roles in impact initiation. Since these reactions could not be distinguished despite the large number of positive correlations that were found, Brill and James argue that correlation studies such as those presented here and in earlier work should not be used for interpretation of mechanistic details.[38] Rather, correlation studies should be used to identify molecular properties that indicate sensitivity to impact. This paper presents such a study.

It has not been until recent years that the molecular properties used in correlation studies could be predicted using accurate quantum mechanical methods. Instead, many of the earlier computational treatments relied on empirical[8−10] or semiempirical[3−5,15−17,19,27] methods. Current computational capabilities and advances in density functional theory[39−41] now allow quantum mechanical molecular characterization to be included in the variety of predictive methodologies used in assessing energetic materials.[26,34] The state of the methods and computers allow for rapid and accurate quantum mechanical calculations of individual energetic molecules, resulting in the capability to predict conformational structures and relative stabilities,[42−44] spectral properties,[44−47] and unimolecular decomposition paths[48−58] of gas-phase energetic materials. Further, many macroscopic properties of bulk energetic materials can be predicted using quantum mechanical information calculated for isolated molecules.[26,59,60] We have been particularly interested in a series of studies by Politzer and co-workers that establish correlations between the features of the quantum-mechanically determined electrostatic potential (ESP) surrounding an isolated molecule and many of its condensed-phase properties.[61−69] For the most part, these studies have correlated attributes of the ESPs of the molecules with bulk properties of materials that are typically associated with intermolecular interactions. Politzer and co-workers have identified a few features of ESPs for CHNO explosives that appear to be related to their sensitivity to impact, a macroscopic property that is not known to be directly dependent on intermolecular interactions in the bulk.[24,25,30−34] In this study, we will expand upon some of the ideas previously presented by calculating and analyzing surface ESPs for a variety of CHNO explosives and identify features common to the various chemical families of CHNO explosives that suggest the degree of sensitivity to impact. Since the calculations presented here will be performed at a higher level of ab initio theory than some of the earlier calculations and for a larger number of explosives, we will also determine whether the previously developed relationships between quantum-mechanically determined features of the ESPs and impact sensitivities are maintained.

Section 2 will provide a review of previous studies that describe relationships between features of the quantum-mechanically predicted ESPs of explosives and their impact sensitivities. Section 3 describes the experimental data that are used in this study to establish the correlations and the quantum mechanical calculations that are performed for each molecule in the experimental set. Section 4 provides a description of the features of the surface ESPs of the explosives under study, and Section 5 examines a variety of parameters that are used to describe features of the surface ESPs. Development and performance of models that relate these parameters to impact sensitivities are also given in this section. Section 5 will also describe limitations in the use of many of these parameters to describe the features of the surface ESPs that are related to the sensitivity of a CHNO explosive. Finally, the summary and conclusions are provided in Section 6.

2. Earlier Studies Relating Molecular Surface ESPs of Explosives to Impact Sensitivities

The electrostatic potential, $V(\mathbf{r})$, is defined as

$$V(\mathbf{r}) = \sum_i \frac{Z_i}{|\mathbf{R}_i - \mathbf{r}|} - \int \frac{\rho(\mathbf{r}')\, d\mathbf{r}'}{|\mathbf{r}' - \mathbf{r}|} \qquad (1)$$

where Z_i and $\mathbf{R}_i$ denote the charge and position of the nucleus of atom i and $\rho(\mathbf{r})$ represents the electronic density. The electrostatic potential is a property that can be determined through diffraction measurements or evaluated using quantum mechanical theory and is often used to analyze the electron density distribution in a molecule. Regions in which the ESP is positive indicate that it is "electron deficient", or that the electron density is low in that area. Regions in which the ESP is negative indicate it is "electron rich", or that the electron density is higher in that region. Thus, ESPs on isosurfaces of electron density are often used in identifying sites within molecules that might be conducive to nucleophilic or electrophilic attack.[30,70,71]

In a quantum mechanical study aimed toward understanding activation or deactivation of the aromatic ring to electrophilic attack through the comparison of calculated ESPs for benzene, nitrobenzene, aniline, and nitroanilines,[30] it was noted that the molecular surface ESPs of the nitroaromatic molecules have positively charged regions over the C−NO_2 bonds. This finding spawned a series of studies that explored this unusual feature[21,22,24,25,31−33] and led Politzer et al. to suggest that the C−NO_2 bond in nitroaromatic systems might serve as a site for nucleophilic attack.[31]

Owens et al.[21] undertook an investigation to address whether the ESP over the C−NO_2 bonding region reflects a degree of instability in the C−NO_2 bond that would subsequently indicate the sensitivity of the explosive. At the time this study was undertaken, the C−NO_2 bonds were believed to be the "trigger linkages" or "seats of thermolytic instability" in this class of explosives.[1,2] The Owens et al. study defined a parameter, V_{Mid}, that estimated the ESP in the C−NO_2 bond region, compared these for a few polynitroaromatic molecules, and explored relations with impact sensitivities. More recently, evidence has been presented that refutes the assumption that the C−NO_2 bond is the trigger linkage in these systems and shows that shock initiation chemistry in nitroarenes proceeds through intermolecular hydrogen atom transfer rather than C−NO_2 scission.[72]

V_{Mid}, an approximation of the ESP at the midpoint of the C−N bond, is defined as

$$V_{Mid} = \frac{Q_C}{0.5R} + \frac{Q_N}{0.5R} \quad (2)$$

where R is the C−NO_2 bond length and the Q_i's (i = C, N) are atomic charges calculated at the Hartree−Fock/STO-3G level.[73] V_{Mid} is not a true representation of the electrostatic potential at the region of interest since it does not include the response of all electrons and nuclei in the molecule. Further, the positive charge buildup that was observed in the region of the C−NO_2 bond was located in planes above the ring rather than along the lines-of-center connecting the nuclei.[30] The Owens et al. study found that measured impact and shock sensitivities of seven polynitroaromatic molecules correlate very well with V_{Mid} for the longest C−NO_2 bond in each molecule.[21] Murray et al.[22] expanded the Owens et al. study by evaluating the V_{Mid} for 26 nitroaromatic molecules. Murray et al. found a good correlation between impact sensitivity measurements and V_{Mid} for 18 nitroaromatics that did not include hydroxynitroaromatic molecules.[22] Politzer and co-workers performed additional studies investigating the relationship between the positive ESPs in the C−NO_2 region of cyclic and acyclic nitro compounds, in an effort to establish if these molecular electronic and structural factors determine a molecule's sensitivity.[24−26,31−34] Included in these are evaluations of the relationship between impact sensitivities for CHNO explosives from different chemical classifications and properties of their ESPs described using a methodology Politzer and co-workers developed to analyze patterns of ESPs on isosurfaces of electron densities of isolated molecules[24,25] This method uses statistically based global quantities to describe charge distributions on the molecular surface ESPs. Correlations between functions using these statistically based quantities and many bulk properties of materials have been established for a variety of properties. The functional descriptions of the various relationships are summarized as a general interaction properties function (GIPF),[65−67] whose form depends on the macroscopic property of interest:

$$\text{Property} = f(\text{SA}, \Pi, \sigma_{Tot}^2, \nu) \quad (3)$$

In this equation, SA, Π, σ_{Tot}^2, and ν are global properties of the ESP on the specified isosurface of electron density. The SA is the molecular surface area of the isosurface of electron density (in all of our calculations, we use the 0.001 electron/bohr^3 isosurface, as recommended by Politzer et al.[65−67]) The statistical quantity Π is the average deviation of $V(\mathbf{r})$ on the molecular surface

$$\Pi = \frac{1}{n}\sum_{i=1}^{n} |V(r_i) - \bar{V}_S| \quad (4)$$

where $V(r_i)$ is the value of the ESP at r_i and $\bar{V}_S$ is the average ESP over the entire isosurface:

$$\bar{V}_S = \frac{1}{n}\sum_{i=1}^{n} V(r_i) \quad (5)$$

Politzer et al. interpret the property Π as representing the degree of charge separation within a molecule.[65−67]

The quantity σ_{Tot}^2 is the total variance of $V(\mathbf{r})$ on the molecular surface and is the sum of the variances σ_+^2 and σ_-^2 defined as

$$\sigma_+^2 = \frac{1}{m}\sum_{i=1}^{m} |V^+(r_i) - \bar{V}_S^+|^2 \quad (6)$$

and

$$\sigma_-^2 = \frac{1}{k}\sum_{i=1}^{k} |V^-(r_i) - \bar{V}_S^-|^2 \quad (7)$$

where $V^+(r_i)$ and $V^-(r_i)$ are positive and negative potential values on the isosurface, respectively, and $\bar{V}_S^+$ and $\bar{V}_S^-$ are the respective averages of the positive and negative regions of the ESP. Politzer et al. describe the parameter σ_{Tot}^2 as providing a measure of the range of values of the surface potential.[65−67] The last quantity, ν, is called the "balance" parameter and is described as showing the degree of balance between the positive and negative potentials on the isosurface:

$$\nu = \frac{\sigma_+^2 \sigma_-^2}{[\sigma_{Tot}^2]^2} \quad (8)$$

This parameter has a maximum value of 0.250 when σ_+^2 equals σ_-^2. Politzer et al. suggest that in this limiting case, the balance parameter indicates that the molecule interacts equally well through either its positive or negative potentials.[65−67] Applications of the GIPF have met with a significant degree of success in predicting a variety of bulk properties, including aqueous solvation free energies, lattice energies in ionic crystals, diffusion coefficients, solubilities, heats of vaporization, sublimation, and fusion, boiling points, partition coefficients, and critical constants.[61−69] Murray, Lane, and Politzer used the GIPF approach to establish correlations between molecular ESPs of CHNO explosives with their impact sensitivities.[24,25]

In the first of the two GIPF applications to this problem,[24] Murray et al. examined the relationship between impact sensitivities and both GIPF global statistical parameters[65−67] and a local parameter, $\bar{V}_{S,max}$, defined as a local maximum on the surface ESP. Using these, a good correlation between ESPs and impact sensitivities of 14 nitroaromatic and 6 nitroheterocyclic molecules was found. Murray et al. found that for the nitroaromatics, the ESP on the surface above the aromatic ring was positive, reflecting the electron-withdrawing effect of the nitro groups. Conversely, in benzene the electrostatic potential in this region is negative. The study showed that the degree of electron deficiency in the region of the delocalized π electrons of the aromatic ring is affected by both electron-withdrawing or -donating substituents attached to the ring. The authors found that the electron donating groups such as NH_2 or OCH_3 partially counteract the electron withdrawing effects of the nitro groups. This counteraction is reflected in both the local quantity $\bar{V}_{S,max}$ and the GIPF parameter Π, interpreted by Murray et al. as the degree of internal charge separation.[24] Three different $\bar{V}_{S,max}$ were examined in this study and correspond to maxima in the electrostatic potential over the C−NO_2 bonds, the substituents H and OH, or over the ring. Murray et al. found that impact sensitivities of the molecules studied had a correlation with the internal charge separation in the molecules (reflected by the global parameter Π) and the local parameter $\bar{V}_{S,max}$(ring), the maximum in the electrostatic potential over the region of the π electrons in the aromatic ring. Murray et al. conclude that since the delocalization of the π electrons in the ring is an important factor in the stability of aromatics, addition of electron withdrawing groups such as NO_2 leads to a removal of the stabilization of the aromatic system.[24] The nitroheterocycles that

were examined are also considered to be aromatic systems but do not share a common structural framework as did the nitroaromatics. The resulting correlation between the parameter Π and impact sensitivities led Murray et al. to conclude that impact sensitivities of explosives within this chemical family are also dependent on the degree of stabilization of the molecule due to charge delocalization.[24]

In the second of the two GIPF applications,[25] these authors examined 13 nitroaromatic, 8 nitramine, and 5 nitroheterocyclic molecules and found that the parameter Π was limited in its ability to predict impact sensitivities for each class of explosives. They were, however, able to establish functional descriptions of the relation between impact sensitivities and properties of the ESPs. Although the functional descriptions of the correlations are different between the classes of explosives, each is a function of parameters that describe the imbalance between the positive and negative regions of the surface ESP. Good correlations were obtained within each of the three classes of explosives using measures of imbalances of the positive and negative ESPs, but a single functional form could not adequately represent the correlations for all three classes.

An ideal predictive methodology using the GIPF variables would be one that could describe the impact sensitivity of any explosive regardless of its chemical classification. In this work, we will attempt to establish such a method by examining possible relationships between GIPF parameters and impact sensitivities for a set of CHNO explosives. The methods will be assessed, and limitations will be described.

3. Details of the Calculations

As noted earlier, there is a concern as to the quality of the drop weight impact measurements to be used in establishing correlations, due to the apparent sensitivity of the results to conditions of the experiment.[1,2,29,36] Therefore, we sought to establish correlations between quantum mechanically calculated properties and measured data for which conditions of the tests were unvarying, well-defined and controlled. One such set of data was found: it consists of drop weight impact test measurements on 39 polynitroaromatic and benzofuroxan molecules.[29] In these tests, significant efforts were made to ensure that the measurements were performed under the same conditions, using the same machine and the same operator.[29] We used molecules from this set to investigate possible relationships between the quantum mechanically calculated properties of the individual molecules with their drop weight impact sensitivities. This set of molecules will be called the "training set".

The training set of molecules consists of a subset of the 39 nitroaromatic or benzofuroxan solid explosives that were evaluated by Wilson et al.[29] Drop weight impact tests were performed for all 39 molecules, but results were reported for only 37. The names of the molecules are given in Table 1, and corresponding two-dimensional structures are illustrated in Appendix A (Supporting Information). We have performed quantum mechanical characterizations for all 39 molecules, which consist of geometry optimizations followed by normal-mode analyses and evaluation of the electron density and electrostatic potential of each molecule at its optimized geometry. All calculations were performed at the B3LYP/6-31G* level.[73,78] The normal-mode analysis for each structure resulted in six zero frequencies and no imaginary frequencies for the remaining vibrational degrees of freedom. This indicates that the structure of each molecule corresponds to a local minimum on the potential energy surface. A search in conformational

TABLE 1: Explosive Compounds Studied[a]

Training Set

compound	chemical name	acronym	$h_{50\%}$ (cm)
1	hexanitrobenzene	HNB	11
2	pentanitrobenzene	PNB	11
3	1,2,3,5-tetranitrobenzene	TetNB	28
4	1,3,5-trinitrobenzene	TNB	71
5	2,4,6-trinitrophenol	picric acid	64
6	pentanitroaniline	PNA	22
7	2,3,4,6-tetranitroaniline	TetNA	47
8	2,4,6-trinitroaniline	TNA	141
9	1,3-diamino-2,4,6-trinitrobenzene	DATB	320[b]
10	1,3,5-triamino-2,4,6-trinitrobenzene	TATB	490[b]
11	2,2′4,4′6,6′-hexanitrobiphenyl	HNBP	70
12	3,3′-diamino-2,2′4,4′,6,6′-hexa-nitrobiphenyl	DIPAM	67
13	4,4′-diamino-2,2′,3,3′,5,5′,6,6′-octanitrobiphenyl	CL-12	20−95
14	2,2′3,3′4,4′5,5′6,6′-decanitro-biphenyl	DNBP	−
15	4,6-dinitrobenzofuroxan	DNBF	76
16	7-amino-4,6-dinitrobenzofuroxan	ADNBF	100
17	5,7-diamino-4,6-dinitrobenzo-furoxan	CL-14	120
18	7-amino-4,5,6-trinitrobenzofuroxan	CL-17	56
19	8-amino-7-nitrobenzobisfuroxan	CL-18	56
20	benzotrifuroxan	BTF	53
21	pentanitrotoluene	PNT	18
22	2,3,4,5-tetranitrotoluene	2,3,4,5-TetNT	15
23	2,3,4,6-tetranitrotoluene	2,3,4,6-TetNT	19
24	2,3,5,6-tetranitrotoluene	2,3,5,6-TetNT	25
25	2,4,6-trinitrotoluene	2,4,6-TNT	98
26	2,3,4-trinitrotoluene	2,3,4-TNT	56
27	3,4,5-trinitrotoluene	3,4,5-TNT	107
28	2-amino-3,4,5,6-tetranitrotoluene	TetN-*o*-Tol	36
29	3-amino-2,4,5,6-tetranitrotoluene	TetN-*m*-Tol	37
30	4-amino-2,3,5,6-tetranitrotoluene	TetN-*p*-Tol	47
31	2,2′,4,4′,6,6′-hexanitrodiphenyl-methane	HNDPM	39
32	2-azido-1,3,5-trinitrobenzene	picryl azide	19
33	azidopentanitrobenzene	CL-16	17
34	2-diazo-4,6-dinitrophenol	DDNP	9
35	5-chloro-2-diazo-4,6-dinitrophenol	5-Cl-DDNP	8
36	3-methyl-2-diazo-4,5,6-trinitro-phenol	Me-NO_2-DDNP	8
37	*N*-methyl-*N*,2,4,6-tetranitroaniline	tetryl	25
38	*N*-methyl-2-amino-*N*,3,4,5,6-pentanitrotoluene	($MeNO_2$N)−22	21
39	*N*-methyl-3-amino-*N*,2,4,5,6-pentanitrotoluene	($MeNO_2$N)−23	18

Test Set

compound	chemical name	acronym	$h_{50\%}$ (cm)
1	tetranitrate pentaerythritol	PETN	13[c]
			16[c]
			12[b]
2	2,4,6,8,10,12-hexanitrohexa-azaisowurtzitane (ϵ-polymorph)	ϵ-CL-20	12[d]
			16[d]
			17[d]
			21[d]
3	2,4,6,8,10,12-hexanitrohexa-azaisowurtzitane (β-polymorph)	β-CL-20	14[d]
4	hexahydro-1,3,5-trinitro-1,3,5-s-triazine	RDX	28[e]
			26[b]
			24[b]
5	1,3,5,7-tetranitro-1,3,5,7-tetraazacyclooctane	HMX	32[d]
			29[b]
			26[b]
6	*N*,*N*′-dinitro-1,2-ethanediamine	EDNA	34[b]
7	2,4,6-trinitroresorcinol	styphnic acid	43[b]
8	2,2′4,4′,6,6′-hexanitrostilbene	HNS	54[e]
9	1,4-dinitroimidazole	dni14	55[f]
10	2,4,5-trinitroimidazole	tri245	68[b]
11	2,4-dinitroimidazole	dni24	105[b]
12	1,1-diamino-2,2-dinitro-ethylene	FOX-7	126[g]
13	2-methoxy-1,3,5-trinitrobenzene	methyl picrate	192[b]
14	3-nitro-1,2,4-triazole-5-one	NTO	291[b]
15	nitroguanidine	NQ	>320[c]

[a] All $h_{50\%}$ values are reported in ref 29 unless otherwise noted. [b] Ref 28. [c] Ref 35. [d] Ref 74. [e] Ref 75. [f] Ref 76. [g] Ref 77.

space for each molecule was not attempted, due to the sizes of some of the molecules. We have assumed, as we did in earlier studies,[59,60] that the energies of the local minima are within a few kcal/mol of the global minimum for each system. The optimized geometry for each molecule was then used to calculate its electron density and electrostatic potential at the B3LYP/6-31G* level. The Gaussian 98 suite of quantum chemistry software[79] and its default settings were used in all calculations.

Although we performed quantum mechanical characterizations for all 39 molecules studied by Wilson et al.,[29] we only used results for 34 of this set in establishing correlations of features of the ESPs with impact sensitivities. Measurements of one system, CL-12, gave widely varying $h_{50\%}$ values that ranged from 20 to 95 cm.[29] For DNBF, no $h_{50\%}$ value was reported.[29] Therefore, we did not include these in this study. Three of the molecules in this set, DNP, 5-Cl-DNP, and Me-NO_2-DNP, are represented by Wilson et al. as zwitterions.[29] Since our quantum mechanical calculations are for isolated molecules, field effects that might induce this dipolar behavior were not modeled. The calculations we performed on these molecules do not show an internal charge separation consistent with zwitterions. Therefore, we have not included these three molecules in this study. Also, Wilson et al. report that DATB and TATB have $h_{50\%}$ values of ">200 cm".[29] We decided that these highly insensitive explosives are important for the parametrization of functions using GIPF parameters; thus, we have used $h_{50\%}$ values measured in other studies for DATB and TATB.[28]

In addition to establishing correlations, we also want to assess the predictive capability of the new models once the correlations are established. To do this, we have chosen a set of CHNO explosives for which drop weight impact test measurements have been performed and applied the new models to them. The identities and drop weight impact test values for this set of molecules (denoted as the "test set") are also given in Table 1, and their structures are illustrated in Appendix B (Supporting Information). The reader will note that several of the molecules in the test set belong to chemical families that differ from the nitroaromatics.

4. Patterns of Charge on the Surface ESPs of Explosives

Before exploring the relationships between the GIPF global parameters and other properties associated with the ESPs, we examined the patterns of the ESPs on the isosurfaces of electron density for the training and test sets of molecules in order to identify potentially distinguishing features of sensitive CHNO explosives. Figure 1 illustrates the electrostatic potentials for the 0.001 electron/bohr^3 isosurface of electron density evaluated at the B3LYP/6-31G* level for several of molecules contained in the training set. In these figures, the colors range from -0.05 to 0.075 hartrees with red denoting extremely electron-deficient regions ($V(\mathbf{r}) > 0.075$ hartree) and blue denoting electron-rich regions ($V(\mathbf{r}) < -0.05$ hartrees). For convenience in analysis, the molecules in Figure 1a−e are grouped according to a base parent structure. The molecules in each group differ only in a few substituents on the aromatic ring. We have also provided a skeletal diagram of each molecule beneath the illustration of its ESP along with its measured $h_{50\%}$ value[29] for the convenience of the reader. Figure 1a compares the patterns of ESPs of polynitrobenzene molecules as a function of the number of NO_2 groups. Figure 1b shows the patterns of polynitroaniline molecules as a function of the number of NO_2 and NH_2 groups on the aromatic ring. Figure 1c illustrates the differences in the ESPs for polynitrobenzofuroxans as a function of NO_2 and NH_2 substituents. Figure 1d shows the ESPs of 2,3,5,6-tetranitrotoluene derivatives as a function of substituent group in the 4th position. Finally, Figure 1e illustrates the ESPs of 1,3,5-trinitrobenzene derivatives as a function of substituent group in the 4th position. In each of these figures, the molecules are illustrated from left to right in order of decreasing sensitivity. The most obvious feature of the ESPs in these figures appears in the region over the aromatic ring. Molecules that are more sensitive to the impact hammer have a larger electron deficiency in this region than molecules that are less sensitive. There also appears to be a deficiency of electron density over the C−N bonding regions in some of the molecules, as observed by Murray et al.[24] Additionally, it seems that the less evenly the electron density is distributed over the body of the molecule (excluding extrema of charge localized over atoms of the electron-donating or electron-withdrawing substituents) the more sensitive the molecule. The effect is most evident in Figure 1a,b, when comparing the least and most sensitive molecules of each series. Figure 2 illustrates the electrostatic potentials of the test molecules, in order of decreasing sensitivity. As seen in the ESPs for the nitroaromatics, the molecules that are more sensitive have significant electron deficiencies within the inner structure of the molecule. Those that are less sensitive do not have these regions of extreme electron deficiencies across the inner frame of the molecule, although some have regions of extreme electron deficiencies at the outer appendages of the molecules (i.e., at H-atom, NH, or NH_2 substituents). An exception is evident in the ESP for 2,4,5-trinitroimidazole (Figure 2). In this case, electron deficient regions appear over the C−N bonds that are adjacent to the NH group. However, the $h_{50\%}$ value for this explosive indicates that it is only moderately sensitive. The next portion of our investigation involves translating these observations into functional descriptions of the distribution of charge that are identified by these ESPs.

5. Development and Performance of Models Using Parameters Related to Features of the Surface ESPs

5.A. Model 1: Positive Charge Buildup over C−NO_2 Bonds. As observed by Murray et al.,[24] the most notable features of the ESPs for the molecules shown in Figure 1 that seem to be related to impact sensitivity are located in the region over the aromatic ring and the C−NO_2 bond regions. Thus, we explored the concept proposed by Owens et al.[21] and Murray et al.[22] regarding the buildup of positive charge over the C−NO_2 bond region and its relation to impact sensitivity. Although our analysis is similar to those of the previous studies,[21,22] we did not use eq 2, which corresponds to the longest of the C−N bonds in the nitroaromatic systems. Rather, we defined an averaged V_{mid}:

$$\bar{V}_{\mathrm{Mid}} = \frac{1}{N}\sum_{i=1}^{N}\left(\frac{Q_{\mathrm{C}}}{0.5R} + \frac{Q_{\mathrm{N}}}{0.5R}\right) \tag{9}$$

in which the summation includes all C−N bonds in the molecule and N denotes the total number of C−N bonds. Also, we did not use the partial charges obtained through Mulliken population analysis that were used in the Murray et al. study.[22] Instead, the partial atomic charges for each molecule were determined by fitting these to the quantum-mechanically derived electrostatic interaction potential surrounding an isolated molecule whose atoms are arranged in the optimized geometry calculated at the B3LYP/6-31G* level. These calculations have been done using the CHELPG procedure as implemented in the Gaussian

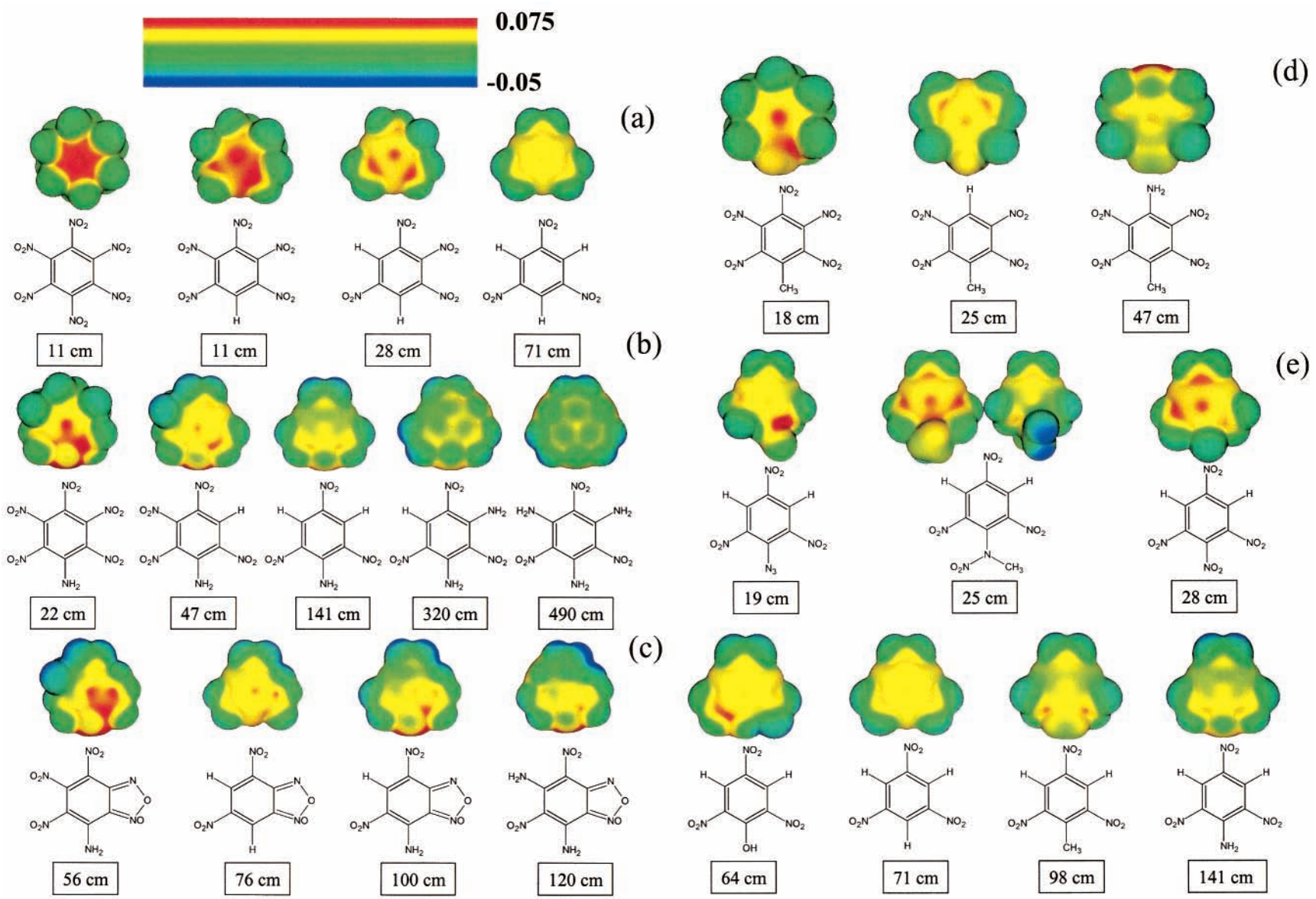

Figure 1. Electrostatic potentials of polynitroaromatic molecules calculated at the B3LYP/6-31G* level. Molecules are grouped according to parent structure, and from left to right, in order of decreasing sensitivity to impact. (a) Hexanitrobenzene, pentanitrobenzene, 1,2,3,5-tetranitrobenzene, and 1,3,5- trinitrobenzene. (b) Pentanitroaniline, 2,3,4,6-tetranitroaniline, 2,4,6-trinitroaniline, 1,3-diamino-2,4,6-trinitrobenzene, and 1,3,5-triamino-2,4,6-trinitrobenzene. (c) 7-Amino-4,5,6-trinitrobenzofuroxan, 4,6-dinitrobenzofuroxan, 7-Amino-4,6-dinitrobenzofuroxan, and 5,7-diamino-4,6-dinitrobenzofuroxan. (d) Pentanitrotoluene, 2,3,5,6-tetranitrotoluene, and 4-Amino-2,3,5,6-tetranitrotoluene. (e) 2-Azido-1,3,5-trinitrobenzene, *N*-methyl-*N*,2,4,6-tetranitroaniline (front and back view), 1,2,3,5-tetranitrobenzene, 2,4,6-trinitrophenol, 1,3,5-trinitrobenzene, 2,4,6-trinitrotoluene, and 2,4,6-trinitroaniline. Measured values of $h_{50\%}$ (ref 28) and two-dimensional structures for each molecule are provided for the reader's convenience. Legend for the color ranges of the ESPs are given above (a) and range from −0.05 (blue) to 0.075 (red) hartrees.

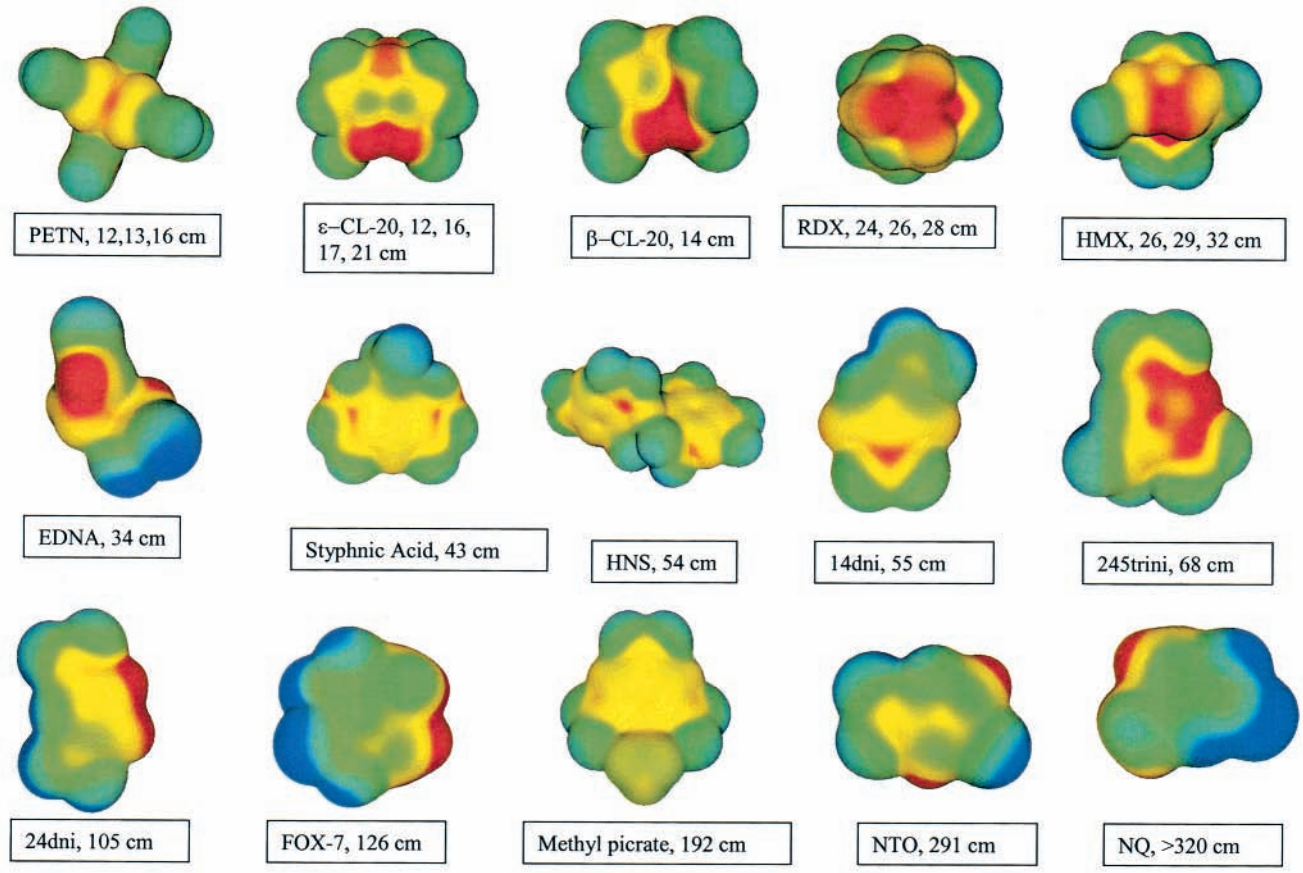

Figure 2. Same as Figure 1, except for the test set of molecules (see Table 1). Two-dimensional structures for each molecule are illustrated in Appendix B (Supporting Information).

98 package.[79] We had hoped to use charges determined using the atoms-in-molecules (AIM) approach.[80] Unfortunately, numerical limitations of the calculations[79] for many of these molecules precluded determination and use of the AIM charges. Also, these numerical limitations prevented evaluation of bond orders in these explosives, thus eliminating any investigation of potential relations between bond order with impact sensitivity.[15−17]

A plot of $\bar{V}_{\mathrm{Mid}}$ calculated using eq 9 versus $h_{50\%}$ values for the training set indicated that no correlation exists between these two properties; rather, the data appeared to be randomly scattered on the figure. We next modified the definition of $\bar{V}_{\mathrm{Mid}}$ to represent the average of the total ESPs calculated at the midpoint of all bonds in each molecule except for the NO bonds in the NO_2 moieties and any X−H bond, (X = O, C, or N). It was hoped that by doing this, we could approximately describe the degree of destabilization of the covalent bonding structure in the inner framework of the molecules, as suggested from the illustrations in Figure 1. In these calculations, the approximate ESP at the midpoint of each bond is evaluated using the partial charges for all atoms in the molecule, as determined using the CHELPG fitting procedure described earlier, rather than only those of the two atoms making up the bond, as in eqs 2 and 9. Thus, this new representation of $\bar{V}_{\mathrm{Mid}}$ is

$$\bar{V}_{\mathrm{Mid}} = \frac{1}{N}\sum_{i=1}^{N}\sum_{j}^{n}\frac{Q_j}{R_{ji}} \qquad (10)$$

where N denotes the number of bonds in the molecule for which the ESPs of the midpoints of the bonds were calculated, n denotes the number of atoms in the molecule, Q_j denotes the partial charge on each atom determined by fitting to the B3LYP/6-31G* ESP as described earlier, and R_{ji} denotes the distance from the midpoint of the ith bond to the jth atom. The $\bar{V}_{\mathrm{Mid}}$ for all molecules in the training and test sets are given in Table 2, and the dependence of the measured $h_{50\%}$ values of the training set to the calculated $\bar{V}_{\mathrm{Mid}}$ is illustrated in Figure 3. This dependence is described by the function (denoted Model 1):

$$h_{50\%} = y_0 + a\exp(-b\bar{V}_{\mathrm{Mid}}) + c\bar{V}_{\mathrm{Mid}} \qquad (11)$$

and best-fit parameters of Model 1 to the $\bar{V}_{\mathrm{Mid}}$ are a = 18922.7503 cm, b = 0.0879 kcal/mol^{-1}, c = −0.3675 cm/kcal/mol, and y_0 = 63.6485 cm. The predictions for Model 1 are illustrated as the solid line in Figure 3, and results are given in Table 3. The correlation coefficient for this fit is 0.96, and the rms deviation of the results from experiment is 26.1 cm. The figure contained in the inset of Figure 3 provides a graphical comparison of the predictions using Model 1 with the experimental $h_{50\%}$ values; a numerical comparison is given in Table 3. The largest deviations of the training set from experiment are the values for DATB and CL-14. The DATB prediction is lower than measured values by 61 kcal/mol, and the prediction for CL-14 is too high by 62 kcal/mol. Application of this model to the test set, however, resulted in extremely poor predictions of impact sensitivities for several of the molecules, particularly for the nitramines. Other representations of $\bar{V}_{\mathrm{Mid}}$ were attempted, which defined $\bar{V}_{\mathrm{Mid}}$ as the averaged value of the ESP at the midpoints of (a) all bonds, (b) only the C−C bonds in the aromatic ring, (c) all C−N and N−N bonds, and (d) all bonds in the molecules except for those within the NH_2 moieties. All of the results were less satisfactory than those of Model 1. Since this model appears to moderately describe nitroaromatics only,

TABLE 2: Quantities Derived from Electrostatic Potentials on the 0.001 au Isosurface of Electron Density

Training Set						
compound	$\bar{V}_{Mid}$ (kcal/mol)	$\bar{V}^+$ (kcal/mol)	$\bar{V}^-$ (kcal/mol)	$\|\bar{V}^+ - \|\bar{V}^-\|\|$ (kcal/mol)	ν	Q (kcal/g)
HNB	136.6	14.2	−4.6	9.5	0.0458	1.642
PNB	125.1	19.4	−6.8	12.6	0.0613	1.530
TetNB	109.4	21.1	−9.4	11.7	0.1159	1.375
TNB	89.0	19.3	−10.3	9.0	0.1884	1.162
picric acid	81.8	19.3	−11.3	8.0	0.1980	1.114
PNA	104.4	22.2	−9.5	12.7	0.0900	1.437
TetNA	88.1	21.5	−12.0	9.5	0.1573	1.272
TNA	65.9	18.7	−12.4	6.3	0.2188	1.051
DATB	51.0	17.3	−13.6	3.7	0.2399	0.964
TATB	42.5	15.5	−14.1	1.4	0.2500	0.908
HNBP	108.0	18.0	−8.4	9.6	0.1524	1.220
DIPAM	87.0	17.0	−10.5	6.5	0.1889	1.113
DNBF	78.3	19.8	−10.9	8.9	0.2029	1.369
ADNBF	67.1	20.5	−14.1	6.4	0.2221	1.224
CL-14	55.9	19.5	−15.5	4.0	0.2483	1.133
CL-17	85.5	22.3	−14.6	7.7	0.1495	1.418
CL-18	65.8	19.9	−13.4	6.5	0.2198	1.385
BTF	72.4	17.6	−7.9	9.7	0.1202	1.653
PNT	110.9	18.5	−7.4	11.0	0.0902	1.413
2,3,4,5-TetNT	92.3	21.8	−10.9	10.9	0.1516	1.267
2,3,4,6-TetNT	94.5	19.8	−9.8	10.0	0.1491	1.257
2,3,5,6-TetNT	97.4	19.4	−9.4	10.0	0.1510	1.258
2,4,6-TNT	74.4	17.7	−10.8	6.9	0.2151	1.044
2,3,4-TNT	66.8	21.0	−15.2	5.8	0.2295	1.088
3,4,5-TNT	71.9	21.7	−15.8	5.9	0.2409	1.078
TetN-*o*-Tol	75.7	24.7	−14.6	10.1	0.1410	1.187
TetN-*m*-Tol	76.9	19.5	−12.2	7.2	0.1878	1.176
TetN-*p*-Tol	77.2	18.5	−11.1	7.4	0.1678	1.183
HNDPM	85.9	18.5	−9.0	9.5	0.1539	1.153
picryl azide	89.7	17.7	−9.7	8.0	0.1754	1.308
CL-16	120.4	16.8	−7.1	9.7	0.0791	1.585
Tetryl	85.8	18.8	−10.5	8.3	0.1784	1.210
($MeNO_2N$)−22	95.5	20.3	−9.3	11.0	0.1220	1.270
($MeNO_2N$)−23	94.4	19.3	−9.8	9.5	0.1608	1.266
Test Set						
compound	$\bar{V}_{Mid}$ (kcal/mol)	$\bar{V}^+$ (kcal/mol)	$\bar{V}^-$ (kcal/mol)	$\|\bar{V}^+ - \|\bar{V}^-\|\|$ (kcal/mol)	ν	Q (kcal/g)
PETN	67.7	17.7	−7.5	10.2	0.1042	1.223
ϵ-CL-20	83.9	21.3	−8.2	13.2	0.0654	1.431
β-CL-20	71.9	20.7	−7.8	12.9	0.0716	1.462
RDX	48.4	21.4	−13.2	8.2	0.1499	1.243
HMX	58.6	23.7	−12.1	11.6	0.1450	1.235
EDNA	33.3	21.7	−14.6	7.1	0.1911	1.005
styphnic acid	75.2	18.6	−11.2	7.4	0.1942	1.063
HNS	80.5	19.2	−9.6	9.6	0.1667	1.151
dni14	69.6	18.2	−14.6	3.6	0.2463	1.276
tni245	115.2	23.1	−11.1	12.0	0.0942	1.414
dni24	75.3	26.0	−16.6	9.4	0.1533	1.155
FOX-7	50.9	24.6	−22.0	2.6	0.1841	1.018
methyl picrate	69.5	17.3	−10.9	6.4	0.2212	1.068
NTO	55.1	22.0	−15.3	6.7	0.1685	0.881
NQ	32.7	26.1	−23.1	3.0	0.2309	0.690

we abandoned this approach. Our next attempts focused on evaluating patterns on the ESPs and developing correlations using expressions that are based on the GIPF methodology as described by Murray et al.[24,25]

5.B. GIPF-Based Parameters Related to Impact Sensitivities. *5.B.1. Models of Murray et al.*[24,25] Application of the GIPF method to the training set of molecules in the manner suggested by Murray et al. in their first study[24] resulted no correlation between the measured and proposed functional description of $h_{50\%}$ values. However, this is not surprising, considering that Murray et al. found these functions had limited utility.[24] GIPF functional relationships for nitroaromatics, nitramines, and nitroheterocycles using global GIPF parameters described in the follow-up study performed by Murray et al.[25] were equally unsuccessful. In the Murray et al. study,[24] the model for nitroaromatics contained both a local and global GIPF parameters. The local GIPF parameter, $\bar{V}_{S,max}$, is defined as the most positive value of the ESP above the aromatic ring. Since we desire a model that is not limited to aromatic systems, we modified the definition for $\bar{V}_{S,max}$ to be the global maximum on the surface ESP. Although this modification of the Murray et al. model did not result in an acceptable predictive model to meet our goals (i.e., a predictive model for all classes of CHNO explosives), the patterns of charge distribution identified by the ESPs of the molecules (Figure 1) indicate that the local GIPF parameter $\bar{V}_{S,max}$ as originally defined in Murray et al.[24] might be an effective parameter describing the degree of sensitivity to impact for nitroaromatic compounds.

We were able to identify two GIPF-based variables that show a correspondence with impact sensitivities. These quantities are given in Table 2 and models for predictions of impact sensitivities using these variables are described in the following two subsections.

5.B.2. Model 2: GIPF Parameters $\bar{V}_S^+$ and $\bar{V}_S^-$. The first statistical quantity that appears to correlate with impact sensitivities of the training set is the difference between the magnitudes of the averages of the positive and negative values of the electrostatic potential on the isosurface, $|\bar{V}_S^+ - |\bar{V}_S^-||$. The trend is illustrated in Figure 4, in which impact sensitivities of the compounds are plotted as a function of this difference. The solid line in this figure shows a nonlinear regression to the function

$$h_{50\%} = a_1 + a_2 \exp[-(a_3|\bar{V}_S^+ - |\bar{V}_S^-||) \qquad (12)$$

where best fit parameters are $a_1 = 9.1949$ cm, $a_2 = 803.4464$

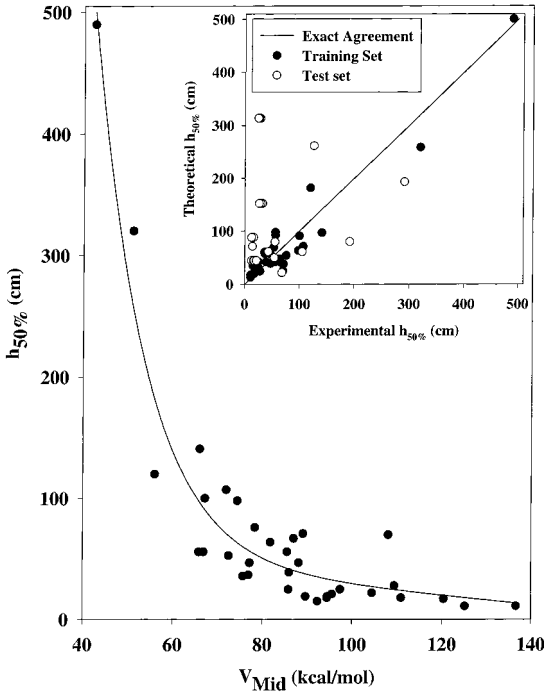

Figure 3. Measured $h_{50\%}$ results vs $\bar{V}_{Mid}$ as defined in eq 10. Predictions using Model 1 [eq 11] are shown as the solid line. Comparison of results using Model 1 to training and test sets of molecules with experimental values are given in the inset.

cm, and $a_3 = 0.3663$ (kcal/mol)$^{-1}$. The correlation coefficient for this fit is 0.94. Values predicted by the model are given in Table 3, and a graphical comparison of the predicted values with experiment are illustrated in the inset of Figure 4. Results for the training set predicted by this model, denoted hereafter as "Model 2", have a rms deviation of 31.2 cm from experiment. The largest deviations of the training set predictions from experiment are for DATB (underestimated by 106 cm) and CL-14 (overestimated by 78 cm). Results from the application of Model 2 to the test set are also given in Table 3 and show a fair description of the more sensitive explosives (with the exception of EDNA). Model 2 performs exceptionally poorly in predicting the impact sensitivities of 1,4-dinitroimidazole, 2,4-dinitroimidazole, FOX-7, and NTO.

5.B.3. Model 3: GIPF Balance Parameter ν. Drop weight impact test data show an approximate exponential growth dependence on another statistical quantity associated with the electrostatic potential of the molecule, the balance parameter, ν, as shown in Figure 5. The solid line in this figure represents the nonlinear least-squares fit of the data to the function

$$h_{50\%} = a_1 + a_2 \exp(a_3 \nu) \tag{13}$$

where $a_1 = 29.3248$ cm, $a_2 = 0.001386$ cm, and $a_3 = 48.8381$. The correlation coefficient for this fit is 0.80, considerably less than that of Models 1 and 2, and the rms deviation of the results from experiment is 54.9 cm. This model significantly underestimates the insensitive explosives DATB and TATB (by 120 and 183 cm, respectively) and greatly overestimates CL-14, 2,3,4-TNT, and 3,4,5-TNT (by 165, 75, and 101 cm, respectively). A graphical comparison of the predictions with experiment is provided in the inset of Figure 5, and a numerical comparison is given in Table 3. The application of this model, denoted as "Model 3" hereafter, to the test set of molecules was disappointing in that it did not show discrimination in impact sensitivities for the sensitive explosives ($h_{50\%} < 30$ cm). Even poorer performance was observed for the more insensitive materials, particularly for 1,4-dinitroimidazole and those with $h_{50\%}$ values > 100 cm.

5.C. Model 4: Heat of Detonation. The formation of hot spots in an explosive is thought to be a key factor in impact initiation and sensitivity of a material. Hot spots are believed to result from any number of causes, including the heat evolved in a localized decomposition reaction within the solid explosive.[1,29,36] As energy release would influence the formation of hot spots, there should be a direct relation between the sensitivity and the heat of reaction of the material. Wu and Fried, in their study of the relation of bond dissociation energies and heats of reactions with the sensitivity of explosives, present results that support this.[13] In that study, Wu and Fried calculated the strengths of the weakest bonds (D_e) in 15 explosives. The findings showed that a strong correlation existed between the $h_{50\%}$ and D_e values for insensitive explosives but the D_e could not be used to discriminate between the sensitive systems. They also evaluated the energy of decomposition (E_d) into equilibrium products at standard state using the Cheetah 2.0 suite of thermochemical codes[81] to assess the relation of E_d with impact sensitivity. The results showed a strong relation between E_d and sensitivity for the more sensitive explosives, whereas E_d was approximately constant for insensitive systems. These two correlations led Wu and Fried to investigate the relationship between sensitivity and the ratio of D_e to E_d.[13] They asserted that D_e is a rough measure of the activation barrier to impact initiation. Once a localized region is ignited, then the localized temperature and subsequent reactions will be controlled by E_d. They contend that since Arrhenius kinetics depend on the ratio of activation barrier to temperature, a relation between sensitivity and the ratio of D_e to E_d might exist. The results showed a strong correlation between this ratio and sensitivity for the range of $h_{50\%}$ values.

The energy content of a material can be determined from the heat of detonation of a material, Q. A quick estimate of the heat of detonation can be obtained from the heat of decomposition of the explosive,[81] defined as

$$Q \cong H_d = \frac{-[\Delta H_f(\text{Detonation products}) - \Delta H_f(\text{Explosive})]}{\text{formula weight of explosive}} \tag{14}$$

The GIPF methodology using quantum mechanical information about a single explosive molecule can be used to evaluate Q.[59,60] In an earlier study, we predicted Heats of Formation for explosives using quantum mechanical (QM) calculations and the GIPF methodology.[59] In a subsequent study, we applied the Kamlet−Jacobs relation and the H_2O-CO_2 arbitrary to predict Heats of Detonation of pure and explosive formulations using predicted Heats of Formation.[60] The Kamlet and Jacobs[82] method assumes that for CHNO explosives, the detonation products correspond to the following decomposition equation, commonly referred to as the H_2O-CO_2 arbitrary:

$$C_aH_bN_cO_d \rightarrow \frac{1}{2}cN_2 + \frac{1}{2}bH_2O + \left(\frac{1}{2}d - \frac{1}{4}b\right)CO_2 + \left(a - \frac{1}{2}d + \frac{1}{4}b\right)C \tag{15}$$

If the heat of formation of the CHNO explosive is known, then using the standard heats of formation for gas-phase water, nitrogen, and carbon dioxide and eq 14 will lead to the prediction of the heat of detonation of an explosive. To demonstrate, Kamlet and Jacobs applied eqs 14 and 15 to 28 pure explosives

TABLE 3: Predicted and Experimental $h_{50\%}$ Values (cm) for Molecules Studied

Training Set						
compound	expt.[a]	$\bar{V}_{Mid}$ Model 1[b]	$V^+ - \lvert\bar{V}^-\rvert$ Model 2[b]	ν Model 3[b]	Q Model 4[b]	Q + ν Model 5[b]
HNB	11	14(−3)	34(−23)	29(−18)	28(−17)	1(10)
PNB	11	18(−7)	17(−6)	29(−18)	28(−17)	2(9)
TetNB	28	25(3)	20(8)	30(−2)	31(−3)	7(21)
TNB	71	38(33)	39(32)	43(28)	56(15)	52(19)
picric acid	64	48(16)	52(12)	51(13)	76(−12)	77(−13)
PNA	22	27(−5)	17(5)	29(−7)	29(−7)	4(18)
TetNA	47	39(8)	34(13)	32(15)	36(11)	19(28)
TNA	141	97(44)	89(52)	90(51)	125(16)	141(0)
DATB	320[c]	259(61)	214(106)	200(120)	283(37)	301(19)
TATB	490[c]	501(−11)	498(−8)	307(183)	502(−12)	478(12)
HNBP	70	25(45)	33(37)	32(38)	43(27)	26(44)
DIPAM	67	41(26)	83(−16)	43(24)	77(−10)	72(−5)
DNBF	76	54(22)	40(36)	57(19)	31(45)	14(62)
ADNBF	100	91(9)	87(13)	100(0)	42(58)	45(55)
CL-14	120	182(−62)	198(−78)	285(−165)	67(53)	102(18)
CL-17	56	43(13)	58(−2)	31(25)	30(26)	7(49)
CL-18	56	98(−42)	84(−28)	93(−37)	30(26)	15(41)
BTF	53	70(−17)	32(21)	30(23)	28(25)	1(52)
PNT	18	24(−6)	23(−5)	29(−11)	30(−12)	4(14)
2,3,4,5-TetNT	15	35(−20)	24(−9)	32(−17)	37(−22)	19(−4)
2,3,4,6-TetNT	19	34(−15)	30(−11)	31(−12)	38(−19)	20(−1)
2,3,5,6-TetNT	25	31(−6)	30(−5)	32(−7)	38(−13)	20(5)
2,4,6-TNT	98	64(34)	73(25)	80(18)	133(−35)	143(−45)
2,3,4-TNT	56	92(−36)	107(−51)	131(−75)	92(−36)	119(−63)
3,4,5-TNT	107	71(36)	103(4)	208(−101)	100(7)	140(−33)
TetN-*o*-Tol	36	60(−24)	29(7)	31(5)	49(−13)	30(6)
TetN-*m*-Tol	37	57(−20)	66(−29)	43(−6)	52(−15)	47(−10)
TetN-*p*-Tol	47	57(−10)	63(−16)	34(13)	50(−3)	38(9)
HNDPM	39	42(−3)	34(5)	32(7)	59(−20)	41(−2)
picryl azide	19	38(−19)	52(−33)	37(−18)	33(−14)	17(2)
CL-16	17	20(−3)	32(−15)	29(−12)	28(−11)	1(16)
tetryl	25	42(−17)	48(−23)	38(−13)	45(−20)	34(−9)
($MeNO_2N$)-22	21	33(−12)	23(−2)	30(−9)	36(−15)	14(7)
($MeNO_2N$)-23	18	34(−16)	34(−16)	33(−15)	37(−19)	20(−2)
rms deviation (cm)		26.1	31.2	54.9	24.1	28.1
Test Set						
compound	expt.	$\bar{V}_{Mid}$ Model 1	$\bar{V}^+ - \lvert\bar{V}^-\rvert$ Model 2	ν Model 3	Q Model 4	Q + ν Model 5
PETN	13[d]	88(−75)	28(−15)	30(−17)	41(−28)	16(−3)
	16[d]	88(−72)	28(−12)	30(−14)	41(−25)	16(0)
	12[c]	88(−76)	28(−16)	30(−18)	41(−29)	16(−4)
ϵ-CL20	12[e]	45(−33)	16(−4)	29(−17)	29(−17)	3(9)
	16[e]	45(−29)	16(0)	29(−13)	29(−13)	3(13)
	17[e]	45(−28)	16(1)	29(−12)	29(−12)	3(14)
	21[e]	45(−24)	16(5)	29(−8)	29(−8)	3(18)
β-CL20	14[e]	71(−57)	16(−2)	29(−15)	29(−15)	3(11)
RDX	28[f]	314(−286)	49(−21)	31(3)	39(−11)	22(6)
	26[c]	314(−288)	49(−23)	31(−5)	39(−13)	22(4)
	24[c]	314(−290)	49(−25)	31(−7)	39(−15)	22(2)
HMX	32[e]	152(−120)	21(11)	31(1)	41(−9)	22(10)
	29[c]	152(−123)	21(8)	31(−2)	41(−12)	22(7)
	26[c]	152(−126)	21(5)	31(−5)	41(−15)	22(4)
EDNA	34[c]	1066(−1032)	69(−35)	45(−11)	190(−156)	153(−119)
styphnic acid	43[c]	62(−19)	62(−19)	48(5)	113(−70)	106(−63)
HNS	54[f]	50(4)	33(21)	34(20)	60(−6)	47(7)
dni14	55[g]	80(−25)	227(−172)	262(−207)	36(19)	38(17)
tni245	68[c]	22(46)	19(49)	29(39)	30(38)	4(64)
dni24	105[c]	61(44)	34(71)	32(73)	59(46)	41(64)
FOX 7	126[h]	262(−136)	320(−194)	40(86)	168(−42)	133(−7)
methyl picrate	192[c]	80(112)	86(106)	98(94)	108(84)	128(64)
NTO	291[c]	193(98)	78(213)	35(256)	668(−377)	296(−5)
NQ	>320[d]	1121(−801)	276(44)	139(181)	5339(−5019)	1800(−1480)

[a] All $h_{50\%}$ values are reported in ref 29 unless otherwise noted. [b] Difference in $h_{50\%}$ values (in cm) given in parentheses. [c] Ref 28. [d] Ref 35 [e] Ref 74. [f] Ref 75. [g] Ref 76. [h] Ref 77.

or explosive formulations and used the resulting heats of detonation to predict the detonation pressures.[82] Their results were in good agreement with values obtained from thermochemical calculations. Our GIPF-based predictions of Q for pure explosives and explosive formulations compared well with experimental values, where known and with values predicted using the well-established thermochemical code Cheetah 2.0[81] and the JCZS-EOS library.[83] Predicted heats of detonation assuming the product H_2O is in the gas phase using QM and Cheetah have rms deviations from experiment of 0.138 and 0.124 kcal/g, respectively. QM predictions assuming the product H_2O is in the liquid phase are in reasonable agreement with measured heats of detonation, with a rms deviation of 0.123 kcal/g from experiment. Also, the QM values for explosive formulations deviated from experiment no more than 0.075 kcal/g. Although the Cheetah calculations have a stronger theoretical basis for prediction of detonation properties,[81] the QM methodology has the advantage that neither heats of formation nor densities needs to be measured or estimated to calculate the heat of detonation of an explosive.

The heats of detonation calculated for the training set of molecules are given in Table 2. The resulting relation between impact sensitivity and the Heats of Detonation of the molecules in the training set is illustrated in Figure 6. A nonlinear least-

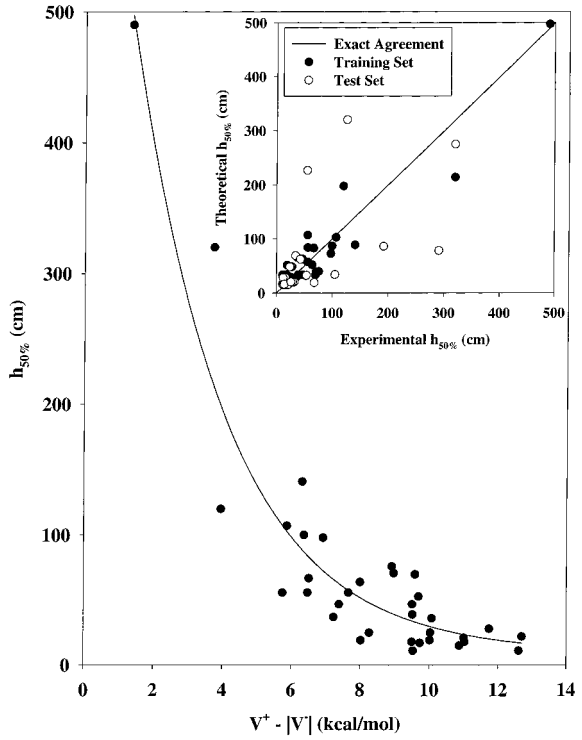

Figure 4. Measured $h_{50\%}$ results vs $|\bar{V}_S^+ - |\bar{V}_S^-||$. Predictions using Model 2 [eq 12] are shown as the solid line. Comparison of results using Model 2 to training and test sets of molecules with experimental values are given in the inset.

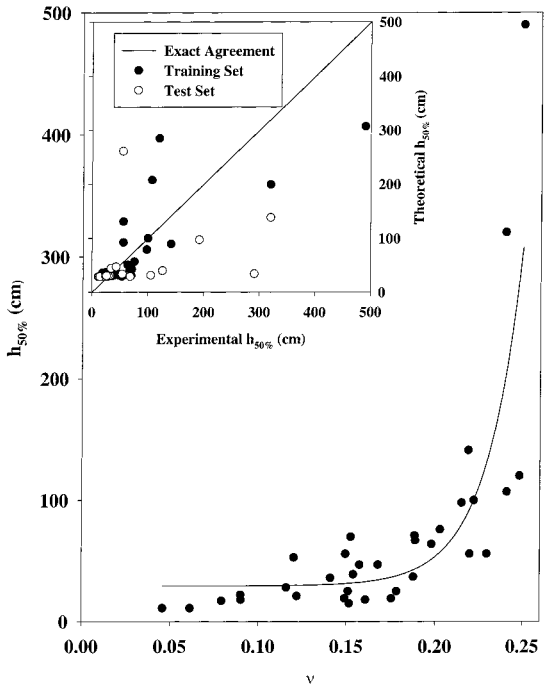

Figure 5. Measured $h_{50\%}$ results vs ν. Predictions using Model 3 [eq 13] are shown as the solid line. Comparison of results using Model 3 to training and test sets of molecules with experimental values are given in the inset.

squares fit of the data to the exponential-decay function

$$h_{50\%} = a_1 + a_2 \exp[-(a_3[Q - a_4])] \qquad (16)$$

is shown as a solid line in the figure. This regression coefficient for this model, denoted as "Model 4" hereafter, is 0.97, and the corresponding parameters are $a_1 = 27.8331$ cm, $a_2 = 0.1135$ cm, $a_3 = 11.0793$ (kcal/g)$^{-1}$, and $a_4 = 1.6606$ kcal/g. Table 3 indicates that the rms deviation of results for Model 4 from experiment is 24.1 cm. Application of Model 4 to the test set of molecules resulted in predictions of $h_{50\%}$ values for several of the explosives being significantly overestimated, especially EDNA, NTO, and NQ.

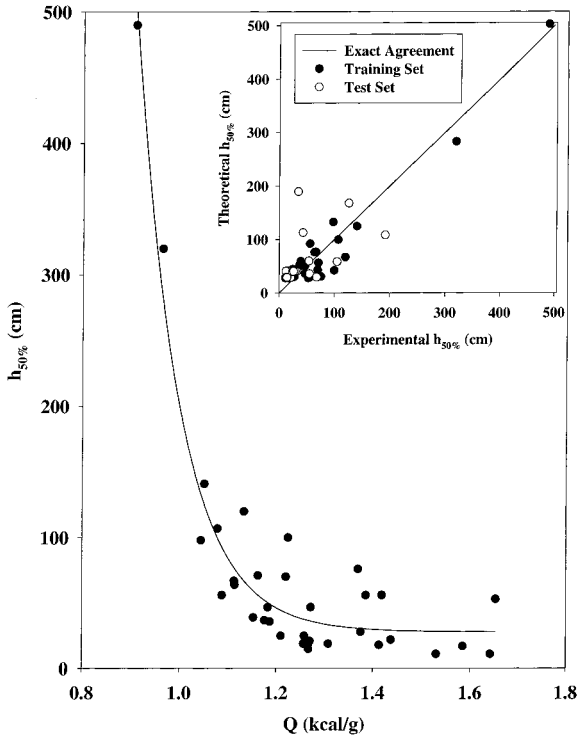

Figure 6. Measured $h_{50\%}$ results vs Q. Predictions using Model 4 [eq 16] are shown as the solid line. Comparison of results using Model 4 to training and test sets of molecules with experimental values are given in the inset.

5.D. Model 5: Hybrid Model Using Q and ν. The identification of molecular parameters that show fair correlations with sensitivity of explosives led to an investigation as to whether hybrid models using some or all of the parameters that individually showed correlations with the experimental $h_{50\%}$ values would improve predictive capabilities. The final model that is considered herein, "Model 5", uses a function that incorporates the heat of detonation with the GIPF balance parameter, ν. This function exhibits the exponential dependencies of both the balance parameter and heats of detonation and has the form

$$h_{50\%} = a_1 \exp(a_2\nu - a_3[Q - a_4]) \qquad (17)$$

Parameters corresponding to the best fit of this function to the data are $a_1 = 1.3410$ cm, $a_2 = 8.1389$, $a_3 = 6.7922$ (kcal/g)$^{-1}$, and $a_4 = 1.4737$ kcal/g. The regression coefficient for this fit is 0.95; comparison of the results with experiment are given in Table 3 and illustrated in Figure 7. The rms deviation of the predictions from the experimental values is 28.1 cm, with the largest deviations being for 2,3,4-TNT (too high by 63 cm) and DNBF (too low by 62 cm). In addition, the model significantly underestimates the $h_{50\%}$ values for all of the benzofuroxans except CL-14. The application of this model to the test set predicted the sensitivities of the majority of the molecules, but greatly overestimated the $h_{50\%}$ values of EDNA and styphnic acid. It also significantly underestimated the $h_{50\%}$ values of 2,4-dinitroimidazole, 2,4,5-trinitroimidazole and methyl picrate. Also, as in Model 4, the $h_{50\%}$ value predicted for nitroguanidine

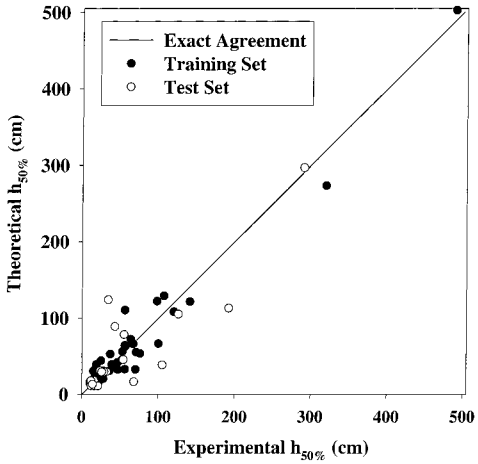

Figure 7. Comparison of results using Model 5 [eq 17] to training and test sets of molecules with experimental values.

is extremely large (1800 cm) and is probably due to the small value of the heat of detonation. Further attempts to fit functions of $\bar{V}_{Mid}$, ν, Q, $|\bar{V}_S^+ - |\bar{V}_S^-||$, and a variety of ratios, products, and sums using combinations of these variables to the training set did not result in improved agreement. Although the hybrid model reasonably predicted sensitivities of many of the explosives in the training and test set over the entire range of values, its failure in several cases indicates that its predictive capabilities are questionable.

5.E. Limitations of the Models for Describing $h_{50\%}$. *5.E.1. Models Using Global GIPF Parameters Only.* The statistical quantities associated with the ESPs that are employed in eqs 12 and 13 had been successfully used in correlating properties dominated by intermolecular interactions of molecules.[61−69] Both variables suggest a role of the degree of imbalance of the positive and negative electrostatic potentials on the sensitivity of a material, as noted by Murray et al. (1998).[25] However, the deficiencies in predictions using Models 2 and 3 suggest that these statistical quantities are inadequate in describing the patterns of charge on the surface ESPs that appear to be related to sensitivity. These statistical quantities describe global charge imbalances but not do depict localized charge imbalances within the molecule that might be related to sensitivity. Local descriptors such as those given for nitroaromatics in Murray et al.[24] might be necessary for developing predictive models of sensitivity.

Examination of the surface ESPs for some of the more insensitive test explosives (2,4-dinitroimidazole, FOX-7, NTO, and NQ; see Figure 2) provide clues to how the definition of the global GIPF parameters might result in inadequate descriptions of charge imbalances could be related to sensitivity. These four systems exhibit large internal charge separations due to charges localized over substituent atoms, whereas it appears from visual examination of the ESPs (Figures 1 and 2) that sensitivity is related to the degree of imbalance of the charge over bonds within the inner skeletal structure of the molecule. For NTO and 2,4-dinitroimidazole, the inner skeletons correspond to the triazole and imidazole ring regions, respectively. For FOX-7 and NQ, the inner skeletons correspond to the ethene and imine parent structures, respectively. For NTO, the ESP over the triazole ring region of the molecule does not indicate the very high electron-deficient regions associated with sensitive explosives. Rather, the extremely electron-rich or electron deficient regions on the surface are localized over the electron-donating or electron-withdrawing substituents. The GIPF parameters as defined in eqs 3−8 cannot distinguish between significant charge separation over an inner structure of a molecule (such as the triazole ring region) versus that due to charge localized on the atoms of the substituents. Since NTO obviously has a large charge separation due to charge localized over the substituent atoms, the parameters ν and $|\bar{V}_S^+ - |\bar{V}_S^-||$ for NTO are comparable to those of more sensitive molecules in the training set (see Figures 4 and 5). Consequently, the resulting predictions of the $h_{50\%}$ values for NTO using both Models 2 and 3 are significantly underestimated. A similar result is found for 2,4-dinitroimidazole, most likely for the same reason as for NTO. FOX-7 and NQ have $|\bar{V}_S^+ - |\bar{V}_S^-||$ and ν values that are consistent with more insensitive molecules, such as DATB and TATB. However, the ESPs illustrated in Figure 2 suggest that the largest contributions to the $|\bar{V}_S^+ - |\bar{V}_S^-||$ and ν parameters are from the charge localized over the NO_2 and NH_2 groups attached to the C−C and C−N double bonds. Since Model 3 does not predict insensitive explosives particularly well, it is not known whether the model itself or an inadequate description of ν for NQ and FOX-7 is the source of the underestimation of the $h_{50\%}$ values for these cases. Also, the $|\bar{V}_S^+ - |\bar{V}_S^-||$ and ν parameters for 1,4-dinitroimidazole is very similar to that of TATB; however, there is a region of significant electron deficiency that appears over the N−NO_2 bond. This localized region of charge imbalance is not well described by these GIPF parameters; thus, its $h_{50\%}$ value is greatly overestimated using Models 2 and 3. Finally, the $h_{50\%}$ value for the moderately sensitive explosive EDNA (34 cm) is overestimated by all of the models, with only Model 3 providing a reasonable prediction (45 cm). The surface ESP for EDNA (Figure 2) illustrates another instance in which extremely positively and negatively charged regions of the ESP are localized over substituent atoms (the oxygen atoms of the NO_2 groups and the hydrogen atom on each of the amine nitrogens). Close examination of the surface ESP indicates the positive charge build-ups over the amine hydrogens extend to the adjacent C−N bonds, perhaps due to repulsive interactions of these hydrogen atoms with the hydrogen atoms of the adjacent methyl group. For systems such as this, the GIPF parameters would reflect mainly the charge build-ups over the substituent atoms rather than any localized charge build-up across adjacent bonds.

5.E.2. Models using Q. The two models in this work that utilize the heat of detonation (Q) predicted using quantum mechanical information and the Kamlet-Jacobs method are limited to the description of CHNO explosives only, since the heats of formation that are used in the evaluation of Q for the systems studied were parametrized using information for systems that contained functional groups common to CHNO explosives. Since predicted heats of formation might have substantial error for systems that are dissimilar from those used in the parametrization of the heats of formation and phase change equations developed in ref 59, such error would be passed along in any ensuing evaluation of Q. For such cases, the accuracy of predictions from the models that use Q could not be assured.

5.E.3. Application of the Models to a Nonexplosive. We investigated whether the models could distinguish between a CHNO explosive and nonexplosive. All of the models in the paper were applied to 3-aminophenol (C_6H_7NO). This system was arbitrarily chosen. The individual molecule was optimized at the same level of theory used for all explosives listed in this study (B3LYP/6-31G*). A subsequent normal-mode analysis confirmed that the optimized structure corresponded to an energy minimum on the potential energy surface. We then evaluated the electrostatic potential and determined point charges centered on each atom that reproduced the electrostatic potential. The

patterns of charge illustrated on the ESP were very similar to that of benzene (completely electronegative over entire aromatic ring; positive charge is localized only on substituent atoms). The following molecular properties pertinent to this study were then generated: $Q = 0$ kcal/g, using a predicted value of heat of formation for the solid of −25.5 kcal/mol from the method described in ref 59. The heat of formation used in the evaluation is poor agreement with experimental values (−47.85 ± 0.29, −46.39 ± 0.24),[84] indicating that error will be propagated through Q. The other GIPF parameters for 3-aminophenol that are necessary to evaluate the impact sensitivity models described in the paper are $|\bar{V}_S^+ - |\bar{V}_S^-|| = 0.6752$ kcal/mol, $\nu = 0.2206$, and $\bar{V}_{Mid} = -53.2$ kcal/mol. We have applied the models to predict of drop weight impact sensitivity for 3-aminophenol. The $h_{50\%}$ values predicted by Models 1, 2, 3, 4, and 5 are 2×10^6 cm, 637 cm, 96 cm, 1×10^7 cm, and 2×10^7 cm, respectively. Thus for a single case, four of the models distinguish between an explosive and a nonexplosive material, but Model 3 predicts an $h_{50\%}$ value within the range of values observed for explosives. This example emphasizes that the balance parameter from the GIPF methodology is limited in its use as a descriptor of sensitivity.

6. Summary and Conclusions

The predictions using three of the models support the Murray et al. observations[24,25] that the impact sensitivity of CHNO explosives have some dependence on the degree of internal charge imbalance within the molecule. We qualify the Murray et al. conclusions in that it appears the charge imbalances that affect sensitivity are associated with localized regions of positive charge build-up over covalent bonds within the molecular frame. For example, the highly insensitive explosives such as TATB, DATB, or nitroguanidine have almost no charge imbalance over the parent structure of the explosive (i.e., the aromatic ring in TATB and DATB). However, there are significant extrema of positive and negative charge localized over the atoms of the substituents, but these extrema do not appear to be related to sensitivity of the explosive. The relationship between these regions of localized charge and sensitivity to impact is not readily described by the global GIPF statistical parameters as defined by Politzer and co-workers.[65−67] Our results showed weak correlations of $h_{50\%}$ values with the GIPF balance parameter ν and with the difference between the magnitudes of the averages of the positive and negative values of the electrostatic potential on the isosurface, $|\bar{V}_S^+ - |\bar{V}_S^-||$. Further, the models using GIPF variables (which were parametrized to describe nitroaromatic explosives) did not adequately predict impact sensitivities for CHNO explosives in other chemical families.

The graphical illustrations of the ESPs (Figures 1 and 2) show that regardless of chemical family of the explosives studied in this work, all of the sensitive molecules have regions of high electron deficiency (>0.075 hartree) over covalent bonds within the inner skeleton of the molecular structure. In the case of the polynitroaromatic explosives, the electron-deficient regions on the surface ESP of sensitive explosives are associated with the delocalized π electrons in the aromatic ring and over the C−N bonds. Since the sensitivities of the molecules under study appear to be related to electron deficiency over covalent bonds within the inner structure of the molecule, the global GIPF parameters could not adequately reflect the localized description of charge buildup that seem to be symptomatic of an explosive's sensitivity.

Finally, there is a dependence of a material's sensitivity to impact with its heat of detonation; however, Q is limited in its utility as a descriptor of sensitivity. We also investigated functions using combinations of the individual GIPF-based variables that showed relationships with impact sensitivities. Our goal was to determine if the combination of parameters would overcome deficiencies in relying on a single parameter in describing the features of charge distribution on the ESPs. Although a resulting hybrid model better predicted the sensitivities of some systems that were inadequately predicted using functions of a single GIPF-based variable, others were very poorly predicted. Thus all models that are presented in this work are limited in their predictive capability.

This work has shown that patterns of charge on the electrostatic potentials for isosurfaces of electron densities surrounding CHNO explosive molecules are useful guides in assessing the degree of sensitivity of a CHNO explosive to impact. Visual examination of these surface potentials show that the most sensitive CHNO explosives have regions of very positive ESPs localized over covalent bonds. This localized region of electron deficiency over covalent bonds is not apparent in the insensitive explosives that were evaluated. Also, this feature in the ESPs of the explosives examined in this study is independent of chemical classification; localized electron deficiencies over covalent bonds were observed in sensitive nitroaromatic, nitrate ester and nitramine systems. However, further studies are needed to determine if these regions of localized electropositive charge reflect chemical instability of the explosive.

Acknowledgment. All calculations were performed at the Army Research Laboratory Major Shared Resource Center, an initiative of the DOD High Performance Computing Modernization Program.

Supporting Information Available: Appendices A and B: names and two-dimensional structures of molecules. This material is available free of charge via the Internet at http://pubs.acs.org.

References and Notes

(1) Kamlet, M. J. *Proc. Symp. Detonation, 6th* **1976**, 312.
(2) Kamlet, M. J.; Adolph, H. G. *Propellants Explos.* **1979**, *4*, 30.
(3) Delpuech, A.; Cherville, J. *Propellants Explos.* **1978**, *3*, 169.
(4) Delpuech, A.; Cherville, J. *Propellants Explos.* **1979**, *4*, 121.
(5) Delpuech, A.; Cherville, J. *Propellants Explos.* **1979**, *4*, 61.
(6) Adolph, H. G.; Holden, J. R.; Cichra, D. A. Technical Report NSWC TR 80-495; Naval Surface Weapons Center: Dahlgren, VA, 1981.
(7) Fukuyama, I.; Ogawa, T.; Miyake, A. *Propellants, Explos., Pyrotech.* **1986**, *11*, 140.
(8) Mullay, J. *Propellants, Explos., Pyrotechn.* **1987**, *12*, 60.
(9) Mullay, J. *Propellants, Explos., Pyrotechn.* **1987**, *12*, 121.
(10) Jain, S. R. *Propellants, Explos., Pyrotechn.* **1987**, *12*, 188.
(11) Fried, L. E.; Ruggiero, A. J. *J. Phys. Chem.* **1994**, *98*, 9786.
(12) McNesby, K. L.; Coffey, C. S. *J. Phys. Chem. B* **1997**, *101*, 3097.
(13) Wu, C. J.; Fried, L. E. *Proc. Symp. Detonation, 6th* **2000**, 490.
(14) Vaullerin, M.; Espagnacq, A.; Morin-Allory, L. *Propellants, Explos., Pyrotech.* **1998**, *23*, 237.
(15) Xiao, H.-M.; Fan, J.-F.; Gu, Z.-M.; Dong, H.-S. *Chem. Phys.* **1998**, *226*, 15.
(16) Fan, J.; Gu, Z.; Xiao, H.; Dong, H. *J. Phys. Org. Chem.* **1998**, *11*, 177.
(17) Fan, J.; Xiao, H. *J. Mol. Struct. (THEOCHEM)* **1996**, *365*, 225.
(18) Zhao-Xu, C.; Heming, X. *Int. J. Quantum Chem.* **2000**, *79*, 350.
(19) Belik, A. V.; Potemkin, V. A.; Sluka, S. N. *Combust., Explos., Shock Waves* **1999**, *35*, 562.
(20) Zeman, S. *Propellants, Explos., Pyrotech.* **2000**, *25*, 66.
(21) Owens, F. J.; Jayasuriya, K.; Abrahmsen, L.; Politzer, P. *Chem. Phys. Lett.* **1985**, *116*, 434.
(22) Murray, J. S.; Lane, P.; Politzer, P.; Bolduc, P. R. *Chem. Phys. Lett.* **1990**, *168*, 135.
(23) Politzer, P.; Murray, J. S.; Lane, P.; Sjoberg, P.; Adolph, H. G. *Chem. Phys. Lett.* **1991**, *181*, 78.
(24) Murray, J. S.; Lane, P.; Politzer, P. *Mol. Phys.* **1995**, *85*, 1.

(25) Murray, J. S.; Lane, P.; Politzer, P. *Mol. Phys.* **1998**, *93*, 187.
(26) Politzer, P.; Alper, H. E. In *Computational Chemistry: Reviews of Current Trends, Vol. 4*, Leszczynski, J., Ed.; World Scientific Publishing Co.: Singapore, 1999.
(27) Owens, F. J. *J. Mol. Struct. (THEOCHEM)* **1996**, *370*, 11.
(28) Storm, C. B.; Stine, J. R.; Kramer, J. F. In *Chemistry and Physics of Energetic Materials*; Bulusu, S. N., Ed.; Kluwer Academic Publishers: Dordrecht, The Netherlands, 1990; pp. 605−639.
(29) Wilson, W. S.; Bliss, D. E.; Christian, S. L.; Knight, D. J. Naval Weapons Center Technical Report NWC TP 7073; 1990.
(30) Politzer, P.; Abrahmsen, L.; Sjoberg, P. *J. Am. Chem. Soc.* **1984**, *106*, 855.
(31) Politzer, P.; Laurence, P. R.; Abrahmsen, L.; Zilles, B. A.; Sjoberg, P. *Chem. Phys. Lett.* **1984**, *111*, 75.
(32) Politzer, P.; Murray, J. S. *J. Mol. Struct.* **1996**, *376*, 419.
(33) Politzer, P.; Murray, J. S. *Mol. Phys.* **1995**, *86*, 251.
(34) Politzer, P.; Murray, J. S. In *Organic Energetic Compounds*; Marinkas, P. L., Ed.; Nova Science Publishers: New York, 1996.
(35) Hall, T. N.; Holden, J. R. Technical Report NSWC MP-88-116; Naval Surface Warfare Center: Dahlgren, VA, 1988.
(36) Bowden, F. P.; Yoffee, A. D. *Initiation and Growth of Explosions in Liquids and Solids*; Cambridge University Press: Cambridge, 1952.
(37) Coffey, C. S.; DeVost, V. F. *Propellants, Explos., Pyrotech.* **1995**, *20*, 105.
(38) Brill, T. B.; James, K. J. *J. Phys. Chem.* **1993**, *97*, 8752.
(39) Chong, D. P., Ed. In *Recent Advances in Density Functional Methods*; World Scientific Publishing Co.: Singapore, 1995; Part I.
(40) Chong, D. P., Ed. In *Recent Advances in Density Functional Methods*; World Scientific Publishing Co.: Singapore, 1997; Part II.
(41) Ziegler, T. *Chem. Rev.* **1991**, *91*, 651.
(42) Harris, N. J.; Lammertsma, K. *J. Am. Chem. Soc.* **1997**, *119*, 6583.
(43) Smith, Grant D.; Bhardwaj, R. K. *J. Phys. Chem. B* **1999**, *103*, 3570.
(44) Rice, B. M.; Chabalowski, C. F. *J. Phys. Chem. A* **1997**, *101*, 8720.
(45) Thompson, C. A.; Rice, J. K.; Russell, T. P.; Seminario, J. M.; Politzer, P. *J. Phys. Chem. A* **1997**, *101*, 7742.
(46) Pati, R.; Das, T. P.; Ray, S. N. *J. Phys. Chem.* **1995**, *99*, 9051.
(47) Pati, R.; Sahoo, N.; Ray, S. N. *J. Phys. Chem. A 101*, 8302.
(48) Politzer, P.; Lane, P.; Redfern, P. C. *J. Mol. Struct.* **1995**, *338*, 249.
(49) Wu, C. J.; Fried, L. E. *J. Phys. Chem. A* **1997**, *101*, 8675.
(50) Politzer, P.; Grice, M. E.; Seminario, J. M. *Int. J. Quantum Chem.* **1997**, *61*, 389.
(51) Politzer, P.; Seminario, J. M.; Zacarias, A. G. *Int. J. Quantum Chem.* **1997**, *64*, 205.
(52) Meredith, C.; Russell, T. P.; Mowrey, R. C.; McDonald, J. R. *J. Phys. Chem. A* **1998**, *102*, 471.
(53) Manaa, M. R.; Fried, L. E. *J. Phys. Chem. A* **1998**, *102*, 9884.
(54) Johnson, M. A.; Truong, T. N. *J. Phys. Chem. A* **1999**, *103*, 8840.
(55) Gindulyte, A.; Massa L.; Huang, L.; Karle, J. *J. Phys. Chem. A* **1999**, *103*, 11045.
(56) Chakraborty, D.; Muller, R. P.; Dasgupta, S.; Goddard, W. A. *J. Phys. Chem. A* **2000**, *104*, 2261.
(57) Lewis, J. P.; Glaesemann, K. R.; Voth, G. A. *J. Phys. Chem. A* **2000**, *104*, 11384.
(58) Chakraborty, D.; Muller, R. P.; Goddard, W. A. *J. Phys. Chem. A* **2001**, *105*, 1302.
(59) Rice, B. M.; Pai, S. V.; Hare, J. *Combust. Flame* **1999**, *118*, 445.
(60) Rice, B. M.; Hare, J. *Thermochem. Acta*, in press.
(61) Murray, J. S.; Fakhr, A.; Politzer, P. *J. Phys. Chem. A* **1999**, *103*, 1853.
(62) Politzer, P.; Murray, J. S.; Flodmark, P. *J. Phys. Chem.* **1996**, *100*, 5538.
(63) Politzer, P.; Lane, P.; Murray, J. S. *J. Phys. Chem.* **1992**, *96*, 7938.
(64) Politzer, P.; Murray, J. S. *J. Phys. Chem. A* **1998**, *102*, 1018.
(65) Politzer, P.; Murray, J. S.; Brinck, T.; Lane, P. In *Immunoanalysis of Agrochemicals*; Nelson, J. O., Karu, A. E., Wong, R. B., Eds.; ACS Symp. Ser. 586; American Chemical Society: Washington, DC, 1994; Chapter 8.
(66) Murray, J. S.; Politzer, P. In *Quantitative Treatment of Solute/Solvent Interactions*; Politzer, P. J., Murray, S., Eds.; *Theoretical and Computational Chemistry*; Elsevier Scientific: Amsterdam, 1994; Vol. 1, pp 243−289.
(67) Murray, J. S.; Brinck, T.; Lane, P.; Paulsen, K.; Politzer, P. *J. Mol. Struct. (THEOCHEM)* **1994**, *307*, 55.
(68) Politzer, P.; Murray, J. S.; Grice, M. E.; DeSalvo, M. E.; Miller, E. *Mol. Phys.* **1998**, *93*, 187.
(69) Politzer, P.; Murray, J. S.; Grice, M. E.; DeSalvo, M. E.; Miller, E. *Mol. Phys.* **1997**, *91*, 923.
(70) Politzer, P.; Landry, S. J.; Warnheim, T. *J. Phys. Chem.* **1982**, *86*, 4767.
(71) Sjoberg, P.; Politzer, P. *J. Phys. Chem.* **1990**, *94*, 3959.
(72) Davis, L. L.; Brower, K. R. *Shock Compression Condens. Mat.* **1997**, 699.
(73) Hehre, W. J.; Radom, L.; Schleyer, P.v. R.; Pople, J. A. *Ab Initio Molecular Orbital Theory*; John Wiley & Sons: New York, 1986; p 271, 298.
(74) Simpson, R. L.; Urtiew, P. A.; Ornellas, D. L.; Moody, G. L.; Scribner, K. J.; Hoffman, D. M. *Propellants, Explos., Pyrotech.* **1997**, *22*, 249.
(75) Dobratz, B. M. Lawrence Livermore National Laboratory Publication UCRL-52997; Lawrence Livermore National Laboratory: Livermore, CA, 1982.
(76) Owens, F. J. Private communication, 2000.
(77) Östmark, H.; Langlet, A.; Bergman, H.; Wingborg, N.; Wellmar, U.; Beem, U. *Proceed. Symp. Detonation, 11th* **1998**, 18.
(78) Becke, A. D. *J. Chem. Phys.* **1993**, *98*, 5648. Lee, C.; Yang, W.; Parr, R. G. *Phys. Rev. B* **1988**, *37*, 785.
(79) Frisch, M. J.; Trucks, G. W.; Schlegel, H. B.; Scuseria, G. E.; Robb, M. A.; Cheeseman, J. R.; Zakrzewski, V. G.; Montgomery, J. A., Jr.; Stratmann, R. E.; Burant, J. C.; Dapprich, S.; Millam, J. M.; Daniels, A. D.; Kudin, K. N.; Strain, M. C.; Farkas, O.; Tomasi, J.; Barone, V.; Cossi, M.; Cammi, R.; Mennucci, B.; Pomelli, C.; Adamo, C.; Clifford, S.; Ochterski, J.; Petersson, G. A.; Ayala, P. Y.; Cui, Q.; Morokuma, K.; Malick, D. K.; Rabuck, A. D.; Raghavachari, K.; Foresman, J. B.; Cioslowski, J.; Ortiz, J. V.; Stefanov, B. B.; Liu, G.; Liashenko, A.; Piskorz, P.; Komaromi, I.; Gomperts, R.; Martin, R. L.; Fox, D. J.; Keith, T.; Al-Laham, M. A.; Peng, C. Y.; Nanayakkara, A.; Gonzalez, C.; Challacombe, M.; Gill, P. M. W.; Johnson, B. G.; Chen, W.; Wong, M. W.; Andres, J. L.; Head-Gordon, M.; Replogle, E. S.; Pople, J. A. *Gaussian 98*, revision A.7; Gaussian, Inc.: Pittsburgh, PA, 1998.
(80) Bader, R. F. W. *Atoms in Molecules: A Quantum Theory*; Oxford University Press: Oxford, 1990.
(81) Fried, L. E.; Howard, W. M.; Souers, P. C. *Cheetah 2.0 User's Manual*; Lawrence Livermore National Laboratory: Livermore, CA, 1998.
(82) Kamlet, M. J.; Jacobs, S. J. *J. Chem. Phys.* **1968**, *48*, 23.
(83) Hobbs, M. L.; Baer, M. R.; McGee, B. C. *Propellants, Explos., Pyrotech.* **1999**, *24*, 269.
(84) NIST Standard Reference Database Number 69, which can be accessed electronically through the NIST Chemistry Web Book (http://webbook/nist/gov/chemistry/); references for all reported data are given there.